DOI: 10.1478/AAPP.96S3A9

AAPP | Atti della Accademia Peloritana dei Pericolanti
Classe di Scienze Fisiche, Matematiche e Naturali
ISSN 1825-1242

Vol. 96, No. S3, A9 (2018)

ECKHAUS AND ZIGZAG INSTABILITY IN A CHEMOTAXIS MODEL OF MULTIPLE SCLEROSIS

ELEONORA BILOTTA [a], FRANCESCO GARGANO [b], VALERIA GIUNTA [c*], MARIA CARMELA LOMBARDO [c], PIETRO PANTANO [a] AND MARCO SAMMARTINO [d]

ABSTRACT. We present a theoretical and numerical study of the bifurcations of the stationary patterns supported by a chemotactic model of Multiple Sclerosis (MS). We derive the normal forms of the dynamics which allows to predict the appearance and stabilization of the emerging branches describing the concentric patterns typical of Balo's sclerosis, a very aggressive variant of MS. Spatial modulation of the Turing-type structures through a zigzag instability is also addressed. The nonlinear stage of the Eckhaus and zigzag instability is investigated numerically: defect-mediated wavenumber adjustments are recovered and the time of occurrence of phase-slips is studied as the system parameters are varied.

1. Introduction

The aim of this paper is to investigate the stability of the stationary patterns supported by a mathematical model of Multiple Sclerosis (MS) proposed in Lombardo *et al.* (2017), which, in its non-dimensional form, reads as:

$$\begin{cases} \frac{\partial m}{\partial t} = \Delta m + m(1-m) - \nabla \cdot \left(\chi \frac{m}{1+m} \nabla c\right), \\ \frac{\partial c}{\partial t} = \frac{1}{\tau}\left[\varepsilon \Delta c + (\delta d - c + \beta m)\right], \\ \frac{\partial d}{\partial t} = rm(1-d)f(m), \qquad \text{with} \quad f(m) = \frac{m}{1+m}. \end{cases} \tag{1}$$

In the above equations m represents the density of the immune cells, c the density of a family of pro-inflammatory cytokines and d represents the density of the damaged oligodendrocytes. The parameter χ represents the maximal chemotactic rate, ε is the diffusivity coefficient of the cytokines, β and δ represent the production rates of the chemical signal by the macrophages and the oligodendrocytes, respectively, τ models the possibility for the cytokine dynamics to evolve on a different time scale compared to the other species, and r represents the maximal destructive strength of the macrophages on the oligodendrocytes. The damaging function f rules the production of apoptotic oligodendrocytes and it has been chosen to be positive and increasing with saturation for high values of the macrophages density.

Using numerical values of the parameters taken from the experimental literature in Lombardo *et al.* (2017) and Bilotta *et al.* (2018), the system (1) has been found to support the formation of stationary patterns that closely reproduce the concentric lesions observed in the clinical practice. However, the weakly nonlinear approach adopted in Lombardo *et al.* (2017) and Bilotta *et al.* (2018) only describes the amplitude and the stability properties of the first bifurcating patterned branch corresponding to the critical mode while fails to account for the pattern selection process. To this end, in this work, we shall focus on the universal secondary instabilities of striped patterns (Hoyle 2006), namely Eckhaus and zigzag, which are longitudinal and transverse instabilities of the primary stationary branches bifurcating from the homogeneous equilibrium. The Eckhaus and zigzag instabilities are at the origin of defect-mediated wavenumber adjustments since they modulate or change the wavelength of the pattern, when it is not optimal. In particular, a perturbation of a striped pattern along the longitudinal direction can generate an Eckhaus instability, which acts on the roll phase to change the wavelength, compressing or dilating the pattern. A perturbation along the transversal direction can excite a zigzag instability, so creating undulations along the rolls.

The motivation for the investigation of the conditions under which such instabilities can be excited relies in that they are known as mechanisms of pattern selection and can account for the formation of defects, frequently reported in real patterns. In fact, both the Eckhaus and the zigzag instability have been the subject of many experimental studies (Lowe and Gollub 1985; Peña *et al.* 2003) and are responsible for the occurrence of several phenomena observed in systems modeled by reaction-diffusion equations, such as the banded vegetation in a semi-arid environment (Dagbovie and Sherratt 2014; Consolo *et al.* 2017), the phase slip and the reversal observed in magnetic fields (Eckmann *et al.* 1995; Pétrélis *et al.* 2015) and the phenomenon of pattern selection in time-growing domains (Knobloch and Krechetnikov 2015; Krechetnikov and Knobloch 2017), just to name a few. An equally important motivation for the interest in the secondary instabilities of Eckhaus-type comes from the fact that, in the case when the primary transition is subcritical, they can account for the birth of localized structures. Analytical studies based on perturbation theory performed on the Swift-Hohenberg equation have indeed revealed a complex bifurcation structure which results in the appearance of homoclinic and heteroclinic snaking branches of localized states, beginning and ending through an Eckhaus bifurcation on primary branches of periodic states (Bergeon *et al.* 2008; Kao and Knobloch 2012). In the context of modeling the demyelinating patterns occurring in MS, this study is therefore a preliminary approach to the investigation of the formation of small localized plaques.

In what follows, adopting a perturbative approach, we shall justify the sequence of successive bifurcations observed in the numerically computed bifurcation diagram of the system (1) in the proximity of the Turing threshold, recovering the numerical bifurcation values of the control parameter and the corresponding stability of the emerging states. This is achieved deriving the amplitude equations of both the Eckhaus and the zigzag instability which capture the stability of the pattern against spatial modulations. In the case of a primary subcritical transition, the theoretical analysis performed shows that the Eckhaus bifurcation, at small amplitudes, is not able to stabilize the emerging periodic branch. This fact is in agreement with the results presented in Bergeon *et al.* (2008) and Kao and Knobloch (2012). Comparison between the theoretical predictions and the

numerical investigations, obtained through direct simulation of the reaction-diffusion-chemotactic system and continuation algorithms, shows an excellent agreement. We have also numerically studied the insurgence of defects determined by phase-slips: in fact, when the established pattern belongs to the Eckhaus unstable region, the wavelength-changing process induces the formation of a singularity, where the amplitude of the pattern vanishes and the phase is undefined. A phase slip then occurs that insert or removes a wavelength into the pattern at the location of the phase slip, originating a new pattern with a different wavelength. We have numerically studied the time needed for a phase slip to occur showing that, for small amplitude perturbations of the pattern, it is entirely determined by the linear growth rate of the instability.

To the best of our knowledge, the Eckhaus bifurcation analysis presented in this paper is the first study on the effects of long-wavelength instabilities performed for a reaction-diffusion-chemotaxis system.

The paper is organized as follows: in Section 2 we shall give the details on the weakly nonlinear analysis performed to obtain the Newell-Whitehead-Segel equation which rules the evolution of the complex amplitude of the pattern. In Section 3 we shall present the study on the onset of the Eckhaus instability in the system (1), in both the supercritical and the subcritical regimes, and we shall show some numerical simulations which support the bifurcation analysis. In Section 4 we shall present the study on the zigzag instability, proving that a finite-size domain results in a stabilizing effect counteracting the instability. Some numerical simulations on 2D domains are also presented. Finally some conclusions are drawn and perspectives for future developments are presented.

2. The Amplitude equation

The system (1) admits three equilibrium points: a disease-free homogeneous state $P_0 \equiv (m_0, c_0, d_0) = (0,0,0)$, and two non-trivial homogeneous equilibria $P_1 \equiv (0, \delta\bar{d}, \bar{d})$, $\forall \bar{d} \in \mathbb{R}_+$, and $P^* \equiv (m^*, c^*, d^*) = (1, \beta+\delta, 1)$. P_0 and P_1 are always unstable, while the stability of P^* depends on the chemotactic parameter χ. Therefore in what follows we shall adopt χ as bifurcation parameter and denote by (χ_c, k_c) the bifurcation threshold of the primary Turing instability and the critical wavenumber, respectively. Their explicit expressions are found to be (Bilotta *et al.* 2018):

$$\chi_c = \frac{2(1+\sqrt{\varepsilon})^2}{\beta}, \qquad k_c^2 = \frac{1}{\sqrt{\varepsilon}}. \tag{2}$$

The homogeneous state P^* is linearly stable for $\chi < \chi_c$. As $\chi \gtrsim \chi_c$, P^* becomes unstable to spatially varying perturbation with most unstable wavenumber k_c.

In this section we shall perform a weakly nonlinear analysis close to the uniform steady state P^* to obtain the equation which rules the amplitude of striped patterns on a rectangular bounded domain $\Omega \subset \mathbb{R}^2$ (Newell and Whitehead 1969). We shall assume, without loss of generality, that the stripes are orthogonal to the x-axis.

Close to the bifurcation threshold, the pattern evolves on slow temporal and spatial scales, therefore we fix the small control parameter $\eta^2 = (\chi - \chi_c)/\chi_c$ and perform a multiple-scale analysis, valid near the threshold ($\eta \ll 1$), using the following slowly varying variables:

$$X = \eta x, \quad Y = \sqrt{\eta} y, \quad T = \eta^2 t. \tag{3}$$

Separating the linear and the nonlinear part, we rewrite the original system (1) in the following way:

$$\partial_t \mathbf{w} = \mathscr{L}^{\chi}\mathbf{w} + \mathscr{N}[\mathbf{w}], \qquad \text{where} \qquad \mathbf{w} = \begin{pmatrix} m-m^* \\ c-c^* \\ d-d^* \end{pmatrix}. \tag{4}$$

The explicit expressions of the linear and nonlinear operators in (4) can be found in Lombardo *et al.* (2017). Close to criticality, one can write the following weakly nonlinear expansion in η:

$$\mathbf{w} = \eta\mathbf{w}_1 + \eta^2\mathbf{w}_2 + \eta^3\mathbf{w}_3 + \cdots, \tag{5}$$

$$\chi = \chi_c + \eta^2\chi_2 + O(\eta^4), \tag{6}$$

so that, following the method adopted in Lombardo *et al.* (2017), one finds the solution at order $O(\eta)$, namely:

$$\mathbf{w}_1 = \boldsymbol{\rho}\left[A(X,Y,T)\,e^{ik_c x} + \bar{A}(X,Y,T)\,e^{-ik_c x}\right], \tag{7}$$

which satisfies the Neumann boundary conditions:

$$\nabla_{\mathbf{x}}\mathbf{w}_1 \cdot \mathbf{n}(\mathbf{x}) = 0, \quad \mathbf{x} \in \partial\Omega \tag{8}$$

where $\mathbf{n}$ denotes the exterior normal to the boundary $\partial\Omega$.

In (7), the vector $\boldsymbol{\rho} \in Ker(\mathscr{L}^{\chi_c})$ is defined up to a constant and A denotes the complex amplitude of the pattern, which evolves according to the following Newell-Whitehead-Segel equation:

$$\frac{\partial A}{\partial T} = \sigma A - \gamma|A|^2 A + \nu^2\left(\partial_X - i\frac{1}{2k_c}\partial_{YY}\right)^2 A, \tag{9}$$

where the explicit expressions of σ, γ and ν in terms of the system parameters are found to be:

$$\sigma = \frac{1+\sqrt{\varepsilon}}{\tau+\sqrt{\varepsilon}}, \quad \gamma = -\frac{(1+\sqrt{\varepsilon})^2(2-55\sqrt{\varepsilon}+63\varepsilon)}{36\beta^2\sqrt{\varepsilon}(\tau+\sqrt{\varepsilon})}, \quad \nu = \frac{4\varepsilon}{(1+\sqrt{\varepsilon})(\tau+\sqrt{\varepsilon})}.$$

3. The Eckhaus instability

In this section we shall study the occurrence of the Eckhaus instability in the system (1). Through the amplitude equation (9) derived in Section **2**, we shall investigate the structure of the bifurcation diagram away from the onset of the primary instability, determining the location of the successive bifurcation points, in both the supercritical ($\gamma > 0$) and the subcritical ($\gamma < 0$) regimes, that present different transition schemes. In the supercritical case, the periodic solutions bifurcate from the trivial state at critical values of the control parameter, above which the newly formed branches inherit the stability properties of the homogeneous state at the bifurcation. In the subcritical regime, periodic solutions bifurcating from the trivial state exist below the thresholds and, by effect of the secondary instabilities, acquire one more unstable direction with respect to the homogeneous state. We shall study these two cases separately.

The Eckhaus instability occurs for perturbations along the longitudinal direction of the stripes, so that, in (9), we can neglect the Y-derivatives, obtaining the following Ginzburg-Landau equation for the amplitude A:

$$\frac{\partial A}{\partial t} = \sigma A - \gamma |A|^2 A + \nu^2 \frac{\partial^2 A}{\partial X^2}, \tag{10}$$

with the corresponding Neumann boundary conditions:

$$\frac{\partial}{\partial x} \Re \left[A(\eta x, t) e^{i k_c x} \right] = 0, \text{ at } x = 0, L. \tag{11}$$

3.1. The supercritical case. In this subsection, we shall study the Eckhaus instability in the supercritical regime and briefly recall the analysis performed in Tuckerman and Barkley (1990).

The amplitude equation (10) can be written in a more convenient form rescaling the variables as follows:

$$\tilde{x} = \frac{\pi}{\eta L} X, \quad \tilde{A} = \frac{\eta L \sqrt{\gamma}}{\pi \nu} A, \quad Q_c = \frac{L}{\pi} k_c, \quad \tilde{t} = \left(\frac{\pi \nu}{\eta L} \right)^2 T, \quad \mu = \sigma \left(\frac{\eta L}{\pi \nu} \right)^2. \tag{12}$$

We therefore obtain the following normalized amplitude equation:

$$\frac{\partial \tilde{A}}{\partial \tilde{t}} = \mu \tilde{A} - |\tilde{A}|^2 \tilde{A} + \frac{\partial^2 \tilde{A}}{\partial \tilde{x}^2}, \tag{13}$$

with Neumann boundary conditions:

$$\frac{\partial}{\partial \tilde{x}} \Re \left[\tilde{A}(\tilde{x}, \tilde{t}) e^{i Q_c \tilde{x}} \right] = 0, \qquad \text{at } \tilde{x} = 0, \pi. \tag{14}$$

Dropping the tildes, the asymptotic solution assumes the following expression:

$$\mathbf{w}(x,t) = 2\eta \Re [A(x,t) e^{i Q_c x}] + O(\eta^2) \tag{15}$$

One solution to (13)-(14) is $A = 0$, which we will call C, or the conductive state.

Looking for solutions of the form $e^{iQx} e^{\lambda t}$ and, by substituting this expression in the linearization of (13), we see that, at $\mu = Q^2$, the state C becomes unstable to an eigenfunction of the form e^{iQx} with eigenvalue $\lambda = \mu - Q^2$.

For $\mu > Q^2$, there exist steady solutions:

$$A = \sqrt{\mu - Q^2} e^{i\phi} e^{iQx}, \tag{16}$$

called "pure modes solutions" and which bifurcate supercritically from the conductive state at $\mu = Q^2$.

For every value of Q, the solution (15), with A given by (16), corresponds to a striped pattern branch with wavenumber $Q_c + Q$. The boundary conditions (14) imply that ϕ can only assume values 0 or π. Thus, for every wavenumber Q, the bifurcation producing the states A is of pitchfork type. Without loss of generality, we will conduct our analysis for $\phi = 0$.

In the finite spatial domain $[0, \pi]$, the wavenumbers are selected by the boundary conditions so that the allowed values of Q are discrete. It is convenient to assign an integer n at each branch A_n, following the ordering of the primary bifurcation points, so that $\mu_n = Q_n^2$ is the $(n+1)$th primary bifurcation encountered as μ increases.

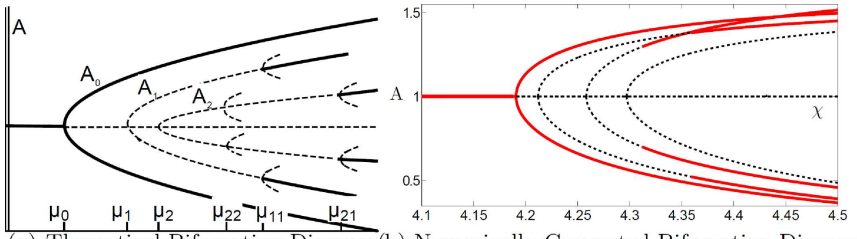

(a) Theoretical Bifurcation Diagram (b) Numerically Computed Bifurcation Diagram

FIGURE 1. (a) Theoretical bifurcation diagram showing the amplitude A of the periodic pattern as the control parameter μ is varied. The solid and dashed portions of the branches represent stable and unstable states, respectively. The branch A_0 is stable at the onset, while the branches A_n, for $n > 0$, are unstable and, as μ increases, undergo n secondary restabilizing bifurcations, the last of which is the Eckhaus bifurcation point. (b) Numerical bifurcation diagram of the system (1) as χ is varied. For the chosen parameter set, namely: $\varepsilon = 0.2$, $\beta = 1$, $\delta = 1$, $\tau = 1$, $r = 1$. The Turing analysis yields a bifurcation value of χ given by $\chi_c = 4.19$ at which a supercritical transition is expected. The solid and dashed portions of the branches represent stable and unstable spatially periodic solutions, respectively.

Through a linear stability analysis (see Tuckerman and Barkley (1990) and Hoyle (2006)), one can prove that the branch A_n, which exists for $\mu > Q_n^2$, is stable if and only if

$$\mu > \mu_E(Q_n) = 3Q_n^2 - \frac{1}{2}. \tag{17}$$

On the other hand, in the case of infinite domain, the solution A is stable if and only if $\mu > \mu_E(Q) = 3Q^2$. Therefore, the finite size of the domain produces a downwards shift of the so called Eckhaus parabola with a consequent stabilizing effect (Kramer and Zimmermann 1985; Ahlers *et al.* 1986; Tuckerman and Barkley 1990): a finite domain creates in fact a "gap" in the (Q,μ)-plane where the Eckhaus instability cannot be excited and whose width includes exactly one allowed wavenumber, namely Q_0. Hence the branch A_0 is always stable at the onset and does not undergo any Eckhaus bifurcation.

Contrarily, the branches A_n, for $n > 0$, are always unstable at the onset: they inherit the instability of the trivial state at $\mu = \mu_n$, and stabilize at the Eckhaus bifurcation point $\mu_E(Q_n)$ (Tuckerman and Barkley 1990).

Through this analysis it is possible to locate the primary and secondary bifurcation points on the bifurcation diagram, whose qualitative appearance is shown in Figure 1(a). Figure1 (b) shows the numerical bifurcation diagram for the system (1) computed using the continuation software AUTO, for $\varepsilon = 0.2$, $\beta = 1$, $\delta = 1$, $\tau = 1$, $r = 1$. For this choice of the parameter values, $\gamma > 0$ and the periodic solution branches bifurcate supercritically from the trivial state. The solid portion of the branches represent stable solutions, while the dashed portions correspond to unstable branches. As predicted by the above analysis, the first branch bifurcating from the conductive state at $\chi = \chi_c = 4.19$ is stable, while the others are unstable and stabilize at the Eckhaus bifurcation points.

3.2. The subcritical case. In this subsection, we shall study the case $\gamma < 0$, in which the branches of periodic solutions bifurcate subcritically from the trivial state.

In the amplitude equation (10) all the variables are rescaled as before, except

$$\tilde{A} = \frac{\eta L\sqrt{-\gamma}}{\pi\nu} A.$$

The following normalized form of the amplitude equation is now recovered:

$$\frac{\partial \tilde{A}}{\partial \tilde{t}} = \mu\tilde{A} + \frac{\partial^2 \tilde{A}}{\partial \tilde{x}^2} + |\tilde{A}|^2\tilde{A}. \tag{18}$$

The boundary conditions and the solution are as in (14) and (15). Proceeding as in the supercritical case, we look for solutions of the form $e^{iQx}e^{\lambda t}$ and find that, at $\mu = Q^2$, the state C becomes unstable to eigenfunctions of the form e^{iQx} with eigenvalue $\lambda = Q^2 - \mu$. For $\mu < Q^2$, the following stationary solutions exist:

$$A = \sqrt{Q^2 - \mu}\, e^{i\phi} e^{iQx}. \tag{19}$$

For every Q, the expression (19) represents two periodic branches which bifurcate from the conductive state C at $\mu = Q^2$ through a subcritical pitchfork bifurcation. As before, we assign an integer n at each branch A_n, following the ordering of the primary bifurcation points $\mu_n = Q_n^2$, and we consider the case $\phi = 0$. To determine the stability of the branch A_n, we perform a linear stability analysis of the perturbed solution $A_n + a$, where

$$a(x,t) = e^{\sigma t} e^{iQ_n x}(\alpha e^{ikx} + \beta e^{-ikx}), \tag{20}$$

with $\alpha, \beta \in \mathbb{R}$ and $k \in \mathbb{Z}^+ - \{0\}$ (we will discuss the case $k = 0$ below).

The eigenvalues have the following expression:

$$\sigma_\pm(Q_n, k, \mu) = Q_n^2 - \mu - k^2 \pm \sqrt{(Q_n^2 - \mu)^2 + (2kQ_n)^2} \qquad \text{for} \quad k \neq 0. \tag{21}$$

Since the eigenvalue $\sigma_-(Q,k,\mu)$ is always negative, the stability of the bifurcating branch A_n depends on $\sigma_+(Q,k,\mu)$. Therefore, the branch A_n is stable for perturbations of the wavenumber if and only if, for all k, $\sigma_+(Q_n,k,\mu) < 0$, or :

$$\mu \geq \sup_{k>0}\left(3Q_n^2 - \frac{k}{2}\right) = 3Q_n^2 - \frac{1}{2} =: \mu_{nE}, \tag{22}$$

where μ_{nE} denotes the Eckhaus bifurcation point on the branch A_n.

Combining (22) with the existence condition $\mu < Q_n^2$, we observe that the branch A_n undergoes an Eckhaus bifurcation if and only if

$$3Q_n^2 - \frac{1}{2} < Q_n^2. \tag{23}$$

The inequality (23) is true if and only if $n < 1$ (in general, it is possible to prove that $3Q_n^2 - \frac{k}{2} < Q_n^2 \Leftrightarrow n < k$, see Tuckerman and Barkley (1990)). Therefore, only the branch A_0 contains the Eckhaus threshold.

The case $k = 0$ corresponds to a perturbation of the amplitude of the pattern. The associated eigenvalue is $\sigma_0 = 2(Q^2 - \mu)$ which, in the subcritical regime, is always positive. Thus the conclusion is that all the bifurcating branches are unstable for perturbations of the amplitude.

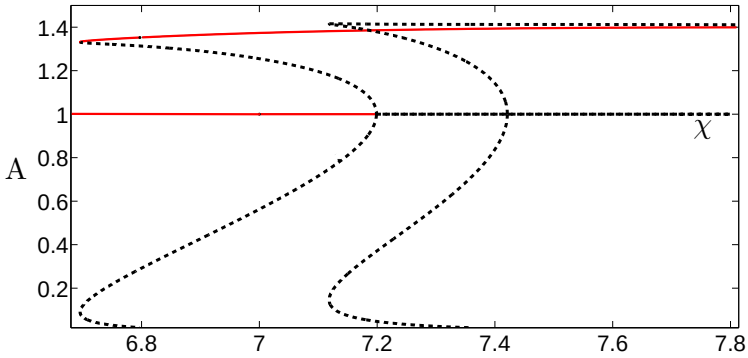

FIGURE 2. Bifurcation diagram of the system (1) as χ is varied. For the chosen parameter values: $\varepsilon = 0.8$, $\beta = 1$, $\delta = 1$, $\tau = 1$, $r = 1$, $\chi_c = 7.18$ and the bifurcations are subcritical. The solid and dashed portions of the branches represent stable and unstable spatially periodic solutions, respectively.

It is worth to stress that this analysis is valid for amplitude of $O(\eta)$, so that any restabilizing bifurcation occurring at large amplitudes has to be described by the quintic Ginzburg-Landau amplitude equation. Figure 2 shows the bifurcation diagram of the system (1) for $\varepsilon = 0.8$, $\beta = 1$, $\delta = 1$, $\tau = 1$, $r = 1$. In agreement with the linear stability analysis, the Turing bifurcation of the first branch occurs at $\chi = \chi_c = 7.18$. For this set of parameters, $\gamma < 0$ and, as predicted by the previous analysis, the branches bifurcate subcritically from the trivial state and they are unstable (dashed portion of the branches). Although the first branch undergoes an Eckhaus bifurcation at small amplitude, it does not stabilize. The stabilization occurs at large amplitude (solid portion of the branch), and then the amplitude equation (18) is not able to predict this bifurcation point.

3.3. Numerical simulations. In this subsection we shall present the results of the numerical investigations we have conducted to validate the analysis exposed above.

Through numerical simulations, we have tested the occurrence of the Eckhaus bifurcation on the branches A_n at $\mu_{nE} = 3Q_n^2 - 1/2$. As the Eckhaus bifurcation point separates the unstable portion of the branch from the stable one, we have fixed a small perturbation of the steady solution (15) as initial condition, both for $\mu < \mu_{nE}$ and for $\mu > \mu_{nE}$: if the branch is unstable, then a modulation of the wavenumber occurs, while if the branch is stable, the perturbation is damped.

We have imposed the homogeneous Neumann boundary conditions to the system (1) on the one-dimensional spatial domain $D = [0, 20\pi]$ ($D = [0, \pi]$ in the rescaled variables defined by (12)), and fixed the values of the dimensionless parameters as given in Table 1, so that the critical wavenumber is $k_c = 1.18921$ (in the rescaled variables $Q_c = 23.7841$) and the primary bifurcation of the Turing branch is supercritical. The boundary conditions on the domain $[0, \pi]$ impose that only integer values of the wavenumber are allowed. Therefore the system will only support periodic pattern whose wavenumber equals $Q_c + Q_n$, for those Q_n such that $Q_c + Q_n$ are integers.

TABLE 1. Non dimensional parameters values used in the numerical simulations. For the chosen set, the primary branch of stationary pattern bifurcates supercritically from the homogeneous state.

Parameter	Description	Value
τ	Time scale of cytokine dynamics	1
ε	Cytokine diffusion	0.5
β	Cytokine production rate	1
δ	Cytokine production rate per olygodendrocyte	1
r	Damaging intensity	1

TABLE 2. Quantities Q_n which differ from $Q_c = 23.7841$ by an integer. They are shown in order of increasing primary bifurcation points $\mu_n = Q_n^2$. The Eckhaus bifurcation values μ_{nE} above which the branch A_n becomes stable are reported in the last column.

n	Q_n	$\mu_n = Q_n^2$	μ_{nE}
0	0.215858	0.0465945	
1	-0.784142	0.614879	1.34464
2	1.21586	1.47831	3.93493
3	-1.78414	3.18316	9.04949
4	2.21586	4.91003	14.2301

In our case, the closest integer to Q_c is 24 and, as $\chi \gtrsim \chi_c = 5.83$, the system selects the pattern with wavenumber $Q_c + Q_0 = 24$, which implies $Q_0 = 0.215858$. In Table (2) the quantities Q_n are reported in their order of bifurcation from the conductive state C. μ_n denotes the primary bifurcation point from which the solution $\mathbf{w}(x,t) = 2\eta\Re\left[\boldsymbol{\rho} A_n e^{iQ_c x}\right] = \eta\Re\left[\boldsymbol{\rho}\sqrt{\mu - Q_n^2} e^{i(Q_c+Q_n)x}\right]$ emerges and μ_{nE} is the Eckhaus bifurcation point, above which the solution stabilizes. We have numerically verified the stability of the branch A_0, setting $\mu > \mu_0$ and assigning a small perturbation of the solution $\mathbf{w}(x,t) = 2\eta\Re\left[\boldsymbol{\rho} A_0 e^{iQ_c x}\right]$ as initial condition. The numerical simulations, not reported here, have confirmed the stability of this branch.

Figure 3(a) and Figure 3(b) show two numerical simulations performed to study the stability properties of the branch A_1. We have set a small perturbation of the solution $\mathbf{w}(x,t) = 2\eta\Re\left[\boldsymbol{\rho} A_1 e^{iQ_c x}\right]$ as initial condition. Figure 3(a) shows the time evolution of the numerical solution for $\mu_1 < \mu < \mu_{1E}$: the system annihilates a roll and the solution falls on the branch A_0. This prove that the branch A_1 is unstable below the Eckhaus bifurcation point, and since the wavenumber is not optimal, the system eliminates a roll in favour of a solution with a more appropriate wavenumber. On the other hand, for $\mu > \mu_{1E}$ the solution with wavenumber 5 becomes stable, as Figure 3(b) shows.

Figure 3(c) and Figure 3(d) show the same analysis conducted on the branch A_2. In both simulations, the initial data is a small random perturbation of the solution on the branch A_2.

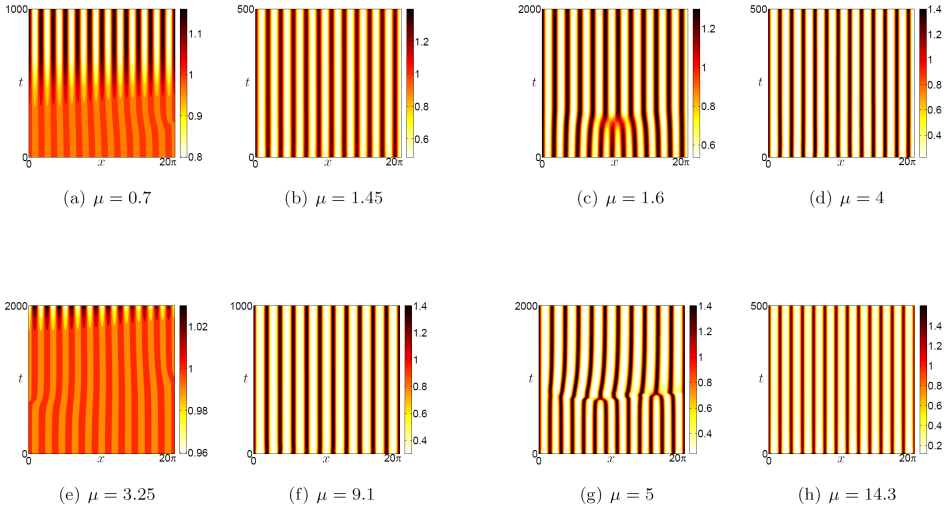

(a) $\mu = 0.7$ (b) $\mu = 1.45$ (c) $\mu = 1.6$ (d) $\mu = 4$

(e) $\mu = 3.25$ (f) $\mu = 9.1$ (g) $\mu = 5$ (h) $\mu = 14.3$

FIGURE 3. Numerical simulations of the macrophage density for the system (1) before and after the Eckhaus bifurcation point. The parameters values are defined in Table 1. In all the displayed figures the initial condition is a small perturbation of the periodic solution A_n. Branch A_1: (a) below and (b) above the Eckhaus bifurcation point. Branch A_2: (c) below and (d) above the Eckhaus bifurcation point. Branch A_3: (e) below and (f) above the Eckhaus bifurcation point. Branch A_4: (g) below and (h) above the Eckhaus bifurcation point.

As it can be seen in Figure 3(c), since the branch A_1 is stable for the selected value of μ, the solution with initial data on A_2 falls on the branch A_1, for $\mu < \mu_{2E}$. While for $\mu > \mu_{2E}$, the solution on the branch A_2 becomes stable and, as shown in Figure 3(d), the perturbation of the solution is damped.

The analysis on the branch A_3 is shown in Figure 3(e), (f): below the Eckhaus bifurcation point, the solution is unstable, indeed we observe a jump on the branch A_1 and after that, although our analysis predict a stable A_1 branch, the solution falls on the branch A_0 (see Figure 3(e)). The numerical simulation in Figure 3(f) confirms that above μ_{2E} the solution becomes stable.

The numerical analysis of the branch A_4 shows similar results: as Figure 3(g) shows, below the Eckhaus bifurcation point μ_{4E} the solution is unstable and falls on the branch A_0, and, as expected, above μ_{4E} the solution becomes stable (Figure 3(h)). We have also investigated how the time to phase slip depends on the linear growth rate σ_+. To ensure that the spectrum of the linearized problem (which depends on ε and β) remains unchanged, we have conducted our analysis fixing the values of $\varepsilon = 0.5$, $\beta = 0.5$, $r = 1, \delta = 1$ and varying the parameter τ. The critical wavenumber is $k_c = 1.18$ which is not allowed by the boundary conditions on the domain $L = [0, 20\pi]$. The selected wavenumber is $\bar{k}_c = 1.20$, which corresponds to a 11-rolls periodic solution. We choose a perturbation of the striped pattern with wavenumber $k = 1.25$ as initial condition, fixing a perturbation with wavenumber $k = 0.05$ and amplitude 0.005. Finally, we have chosen the value of $\chi = 11.714$, which

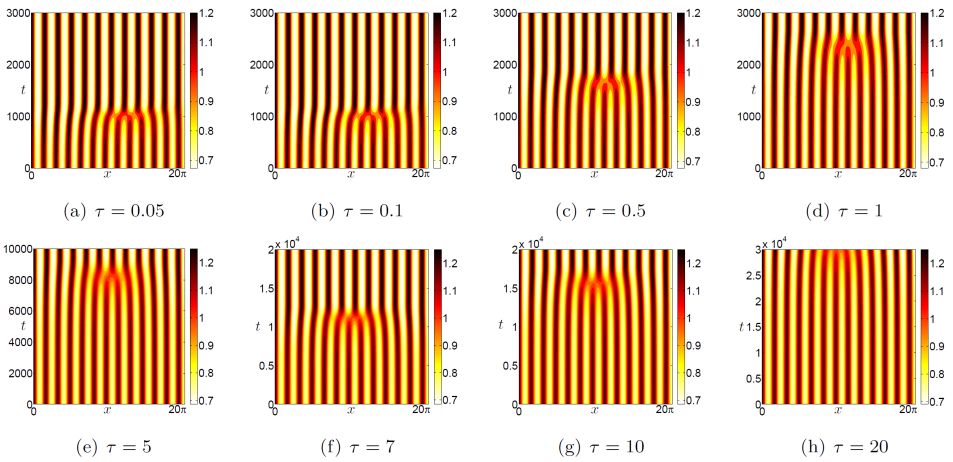

(a) $\tau = 0.05$ (b) $\tau = 0.1$ (c) $\tau = 0.5$ (d) $\tau = 1$

(e) $\tau = 5$ (f) $\tau = 7$ (g) $\tau = 10$ (h) $\tau = 20$

FIGURE 4. Time evolution of the numerical solution of the system (1) in a domain of size $L = 20\pi$ for different values of τ. In each simulation, the initial condition is a perturbation of the striped pattern with wavenumber $k = 1.25$. To observe the phenomenon of phase slip the bifurcation parameter χ is chosen in the Eckhaus unstable region.

lies in the Eckhaus unstable region, so that the initial perturbation triggers the phase slip of the solution. The results of the numerical experiments are reported in Figure 4 where one can see that the time of the phase slip is an increasing function of τ. We recall here that the parameter τ is a measure of the characteristic time scale of the cytokines dynamics and that, as reported in Lombardo *et al.* (2017), biologically meaningful values of τ lie in the interval $[10^{-3}, 1]$. Therefore, for small values of τ, the Eckhaus instability can be an effector mechanism of wavelength selection on the emerging demyelinating pattern.

Finally we have quantitatively investigated the dependence of the time to phase slip on the linear growth rate of the instability: in Figure 5 we have plotted $log(T_{slip})$ as a function of $-log(\sigma_+)$, using the values reported in Table 3. The resulting graph is a straight line of unit slope, indicating that, for the chosen small amplitude initial perturbations, the time to phase slip is entirely determined by the linear growth rate σ_+. Qualitatively similar results have been obtained in Kao and Knobloch (2012), in the study of the phase slips induced by the Eckhaus instability of weakly subcritical patterns of the Swift-Hohenberg equation.

4. The zigzag instability

In this section we shall study the onset of zigzag instabilities in the system (1) and we shall also prove the stabilizing effects of a finite domain. The zigzag instability occurs for perturbation along the transversal direction of the stripes, then in this case the amplitude equation is (9).

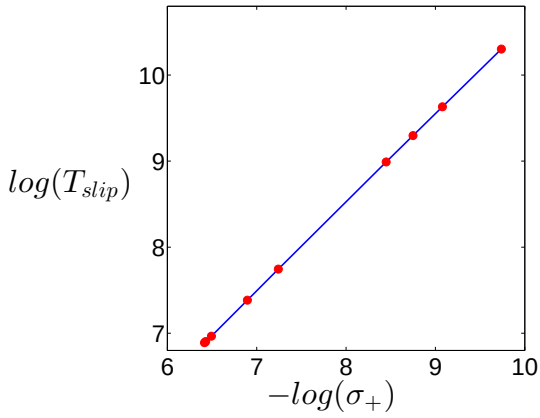

FIGURE 5. $log(T_{slip})$ as a function of $-log(\sigma_+)$: the plot is a straight line of unit slope.

TABLE 3. Values of σ_+ and T_{slip} corresponding to the different values of τ in the numerical simulations shown in Figure 4.

τ	σ_+	T_{slip}
0.05	1.16×10^{-3}	995
0.1	1.15×10^{-3}	1060
0.5	1.01×10^{-3}	1610
1	7.16×10^{-4}	2310
5	2.14×10^{-4}	8023
7	1.59×10^{-4}	10906
10	1.14×10^{-4}	15230
20	5.90×10^{-5}	27900

As before, we rescale all the variables to obtain the following normalized form of the amplitude equation:

$$\frac{\partial A}{\partial t} = \mu A - |A|^2 A + \left(\partial_x A - i\frac{1}{2k_c}\partial_{yy} A\right)^2, \tag{24}$$

and, imposing Neumann boundary conditions, it is easy to verify that one solution to (24) is $A = 0$. Looking for solutions of the form $e^{iQx}e^{\lambda t}$ and substituting this expression into (24), we see that at $\mu = Q^2$ the state C becomes unstable to an eigenfunction of the form e^{iQx} with eigenvalue $\lambda = \mu - Q^2$.

As before, for $\mu > Q^2$ there exist the steady solutions:

$$A_\infty = \sqrt{\mu - Q^2}\, e^{iQx}. \tag{25}$$

To determine the stability of the solutions A_∞, we add a perturbation of the form

$$a(x,y,t) = e^{\sigma t} e^{iQx}(\alpha e^{iPy} + \beta e^{-iPy}), \tag{26}$$

TABLE 4. Non dimensional parameters values used in the numerical simulations

Parameter	Description	Value
τ	Time scale of cytokine dynamics	1
ε	Cytokine diffusion	0.55
β	Cytokine production rate	1
δ	Cytokine production rate per olygodendrocyte	1
r	Damaging intensity	1

with α and β real. By substituting $A_\infty + a$ in (24) and neglecting the nonlinear terms in a, we derive the following equation for a:

$$\sigma a = \mu a - 2|A_\infty|^2 a - (A_\infty)^2 a^* + \left(\partial_x - i\frac{1}{2k_c}\partial_{yy}\right)^2 a. \tag{27}$$

Inserting the expression (26) into (27) and equating to zero the coefficients of $e^{i(Qx+Py)}$ and $e^{i(Qx-Py)}$, we get the following eigenvalue problem:

$$\begin{pmatrix} \sigma & 0 \\ 0 & \sigma \end{pmatrix} \begin{pmatrix} \alpha \\ \beta \end{pmatrix} = \begin{pmatrix} -\mu + Q^2 - \frac{QP^2}{k_c} - \frac{P^4}{4k_c^2} & -\mu + Q^2 \\ -\mu + Q^2 & -\mu + Q^2 - \frac{QP^2}{k_c} - \frac{P^4}{4k_c^2} \end{pmatrix} \tag{28}$$

from which we obtain the eigenvalues:

$$\sigma_1 = -P^2\frac{P^2 + 4k_cQ}{4k_c^2}, \qquad \sigma_2 = -P^2\frac{P^2 + 4k_cQ}{4k_c^2} - 2(\mu - Q^2). \tag{29}$$

Imposing $\sigma_1 < 0$, we get the condition $Q > -\frac{P^2}{4k_c}$. Therefore, the branch A_∞ is stable if and only if $Q > -\frac{P^2}{4k_c}$, for every admitted value of P, and, therefore, if and only if:

$$Q > \min_{P>0}\left(-\frac{P^2}{4k_c}\right). \tag{30}$$

The boundary conditions impose that P is a integer so that the branch A_∞ is zigzag unstable if the following condition holds:

$$Q < -\frac{1}{4k_c}. \tag{31}$$

On the other hand, in the case of a domain of infinite length P can be any nonzero real number and, in the limit of P tending to 0, the condition for the zigzag instability is $Q < 0$. We have then proved that a the finite domain has a stabilizing effect, in the sense that it shifts to the left the region of stable modes (Figure 6).

Figure 7 shows the time evolution of a numerical solution obtained fixing the following values for the parameters: The domain is $[0, 20\pi] \times [0, 20\pi]$ and we have imposed homogeneous Neumann boundary conditions. The critical wavenumber is $Q_c = 23.2241$. We have fixed as initial condition a small perturbation of the branch A_0 along the y-axis to test the stability of the branch $A_0 = \sqrt{\mu - Q_0^2}e^{iQ_0x}$, where $Q_0 = -0.2241$.

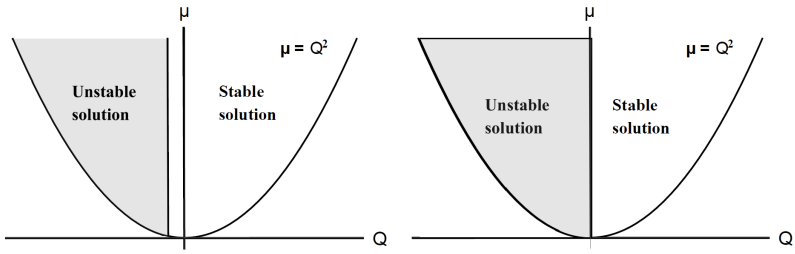

(a) Finite domain (b) Infinite domain

FIGURE 6. Zigzag instability regions in: (a) finite domains and (b) infinite domains. Above the curve $\mu = Q^2$, the stationary solution $A = \sqrt{\mu - Q^2}e^{iQx}$ exists. The stable region is shifted to the left by the stabilizing effect of the finite domain.

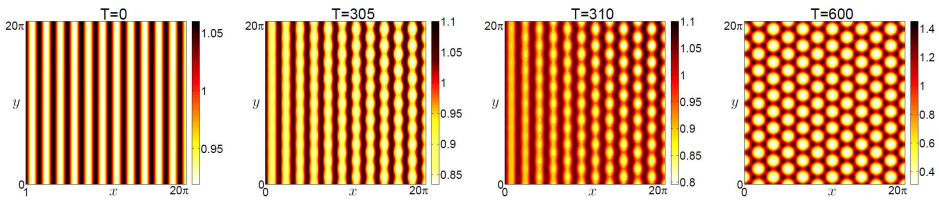

(a) (b) (c) (d)

FIGURE 7. Temporal evolution of the numerical simulations on the branch A_0, which is zigzag unstable. The figures show the macrophage density for the system (1). The initial condition is a small perturbation of the periodic solution along the y-axis. The parameters values are defined in Table 4

The condition for the zigzag instability holds and, as predicted by the previous analysis, the solution, after a long transient in which the solution seems to have reached a steady state, shows undulations along the rolls (Figure 7(b)). The undulation are soon more stressed (Figure 7 (c)) and finally the solution evolves towards a stationary hexagonal pattern (Figure 7 (d)). The transition, excited by the zigzag instability, from unstable striped pattern to hexagons can be described through a stability analysis of the phase equation (Ghoniem and Walgraef 2008) and will be addressed in a forthcoming paper.

5. Conclusions

The mathematical description of the pathological features of Multiple Sclerosis has recently attracted much attention (Calvez and Khonsari 2008; Kotelnikova *et al.* 2017a,b; Lombardo *et al.* 2017; Akaishi *et al.* 2018). In this paper we have described the dynamical transitions induced by long-wavelength instabilities on the stationary extended patterns supported by a reaction-diffusion-chemotaxis model of Multiple Sclerosis. Several problems remain to be discussed.

The Eckhaus instability results in the exponential growth of the wavenumber modulations and, when nonlinearities come into effect, in a wavelength selection mechanism mediated by moving dislocations. As the proposed model admits two dimensional periodic patterns resembling the concentric demyelinating structures typical of Balò Sclerosis, it would be of interest to investigate the appearance and the interaction of two-dimensional defects, which could realistically reproduce the patterns observed in the MRIs of MS patients.

The numerical investigation of the Turing-type branches emerging from the homogeneous equilibrium performed in Lombardo *et al.* (2017) on one-dimensional domains has revealed, far from the primary bifurcation, an Eckhaus scenario, followed by a Andronov-Hopf bifurcation, which determines the appearance of an oscillating pattern. As the control parameter is further increased, a second incommensurate frequency develops and spatio-temporal chaotic dynamics is observed (Abdechiri *et al.* 2017). A similar route to chaos through quasiperiodicity has been recently reported in reaction-diffusion systems (Tulumello *et al.* 2014; Périnet *et al.* 2017; Gambino *et al.* 2018) and is believed to be a robust mechanism of destabilization for extended systems in nature (Clerc and Verschueren 2013). The detailed investigation of this scenario for the present model will be the subject of a forthcoming paper.

Another important point that deserves attention is the description of small localized zone of demyelinating activity, which are frequently recorded in the MS pathology. This phenomenon could be accounted for by the formation of localized dissipative structures, usually found in reaction-diffusion systems far from equilibrium. These states are organized in a homoclinic snaking bifurcation structure, where the snaking branches bifurcate subcritically from the Turing branch through an Eckhaus instability (Parra-Rivas *et al.* 2018). A precise understanding of the organization of localized states in a homoclinic snaking structure for the model proposed here will be treated in the future.

Finally an Eckhaus and zigzag bifurcation analysis performed on reaction-diffusion systems supporting the formation of different planar structures (Gambino *et al.* 2014; Bozzini *et al.* 2015) would allow the exploration of the parameter regimes under which point defects or subdomains with different orientations are triggered (Sushchik and Tsimring 1994; Tsimring 1996; Pezzutti *et al.* 2011). This is an issue of relevance for many applicative fields and will be addressed elsewhere.

Acknowledgments

The authors acknowledge the financial support of GNFM-INdAM. The work of F.G. and V.G. has been supported by a Progetto Giovani grant.

References

Abdechiri, M., Faez, K., Amindavar, H., and Bilotta, E. (2017). "The chaotic dynamics of high-dimensional systems". *Nonlinear Dynamics* **87**(4), 2597–2610. DOI: 10.1007/s11071-016-3213-3.

Ahlers, G., Cannell, D. S., Dominguez-Lerma, M. A., and Heinrichs, R. (1986). "Wavenumber selection and Eckhaus instability in Couette-Taylor flow". *Physica D: Nonlinear Phenomena* **23**(1-3), 202–219. DOI: 10.1016/0167-2789(86)90129-6.

Akaishi, T., Takahashi, T., and Nakashima, I. (2018). "Chaos theory for clinical manifestations in Multiple Sclerosis". *Medical hypotheses* **115**(4), 87–93. DOI: 10.1016/j.mehy.2018.04.004.

Bergeon, A., Burke, J., Knobloch, E., and Mercader, I. (2008). "Eckhaus instability and homoclinic snaking". *Physical Review E* **78**(4), 046201. DOI: 10.1103/PhysRevE.78.046201.

Bilotta, E., Gargano, F., Giunta, V., Lombardo, M. C., Pantano, P., and Sammartino, M. (2018). "Axisymmetric solutions for a chemotaxis model of Multiple Sclerosis". *Ricerche di Matematica* (in press), 1–14. DOI: 10.1007/s11587-018-0406-8.

Bozzini, B., Gambino, G., Lacitignola, D., Lupo, S., Sammartino, M., and Sgura, I. (2015). "Weakly nonlinear analysis of Turing patterns in a morphochemical model for metal growth". *Computers and Mathematics with Applications* **70**(8), 1948–1969. DOI: 10.1016/j.camwa.2015.08.019.

Calvez, V. and Khonsari, R. H. (2008). "Mathematical description of concentric demyelination in the human brain: Self-organization models, from Liesegang rings to chemotaxis". *Mathematical and Computer Modelling* **47**(7-8), 726–742. DOI: 10.1016/j.mcm.2007.06.011.

Clerc, M. G. and Verschueren, N. (2013). "Quasiperiodicity route to spatiotemporal chaos in one-dimensional pattern-forming systems". *Physical Review E - Statistical, Nonlinear, and Soft Matter Physics* **88**(5), 052916. DOI: 10.1103/PhysRevE.88.052916.

Consolo, G., Currò, C., and Valenti, G. (2017). "Pattern formation and modulation in a hyperbolic vegetation model for semiarid environments". *Applied Mathematical Modelling* **43**, 372–392. DOI: 10.1016/j.apm.2016.11.031.

Dagbovie, A. S. and Sherratt, J. A. (2014). "Pattern selection and hysteresis in the Rietkerk model for banded vegetation in semi-arid environments". *Journal of The Royal Society Interface* **11**(99), 20140465. DOI: 10.1098/rsif.2014.0465.

Eckmann, J. P., Gallay, T., and Wayne, C. E. (1995). "Phase slips and the Eckhaus instability". *Nonlinearity* **8**(6), 943–961. DOI: 10.1088/0951-7715/8/6/004.

Gambino, G., Lombardo, M. C., and Sammartino, M. (2014). "Turing instability and pattern formation for the Lengyel-Epstein system with nonlinear diffusion". *Acta Applicandae Mathematicae* **132**(1), 283–294. DOI: 10.1007/s10440-014-9903-2.

Gambino, G., Lombardo, M. C., and Sammartino, M. (2018). "Cross-diffusion-induced subharmonic spatial resonances in a predator-prey system". *Physical Review E - Statistical, Nonlinear, and Soft Matter Physics* **97**(1), 012220. DOI: 10.1103/PhysRevE.97.012220.

Ghoniem, N. and Walgraef, D. (2008). *Instabilities and self organization in materials*. Oxford Univ. Press. DOI: 10.1093/acprof:oso/9780199298686.001.0001.

Hoyle, R. B. (2006). *Pattern formation: an introduction to methods*. Cambridge University Press. DOI: 10.1063/1.2774102.

Kao, H. C. and Knobloch, E. (2012). "Weakly subcritical stationary patterns: Eckhaus instability and homoclinic snaking". *Physical Review E - Statistical, Nonlinear, and Soft Matter Physics* **85**(2), 026211. DOI: 10.1103/PhysRevE.85.026211.

Knobloch, E. and Krechetnikov, R. (2015). "Problems on time-varying domains: Formulation, dynamics, and challenges". *Acta Applicandae Mathematicae* **137**(1), 123–157. DOI: 10.1007/s10440-014-9993-x.

Kotelnikova, E., Kiani, N. A., Abad, E., Martinez-Lapiscina, E. H., Andorra, M., Zubizarreta, I., Pulido-Valdeolivas, I., Pertsovskaya, I., Alexopoulos, L. G., Olsson, T., Roland, M., Friedemann, P., Jesper, T., Jordi, G. O., and Pablo, V. (2017a). "Dynamics and heterogeneity of brain damage in multiple sclerosis". *PLoS computational biology* **13**(10), e1005757. DOI: 10.1371/journal.pcbi.1005757.

Kotelnikova, E., Zubizarreta, I., Pulido-Valdeolivas, I., and Villoslada, P. (2017b). "Systems medicine modeling for multiple sclerosis". *Current Opinion in Systems Biology* **3**, 125–131. DOI: 10.1016/j.coisb.2017.05.002.

Kramer, L. and Zimmermann, W. (1985). "On the Eckhaus instability for spatially periodic patterns". *Physica D: Nonlinear Phenomena* **16**(2), 221–232. DOI: 10.1016/0167-2789(85)90059-4.

Krechetnikov, R. and Knobloch, E. (2017). "Stability on time-dependent domains: convective and dilution effects". *Physica D: Nonlinear Phenomena* **342**, 16–23. DOI: 10.1016/j.physd.2016.10.003.

Lombardo, M. C., Barresi, R., Bilotta, E., Gargano, F., Pantano, P., and Sammartino, M. (2017). "Demyelination patterns in a mathematical model of multiple sclerosis". *Journal of Mathematical Biology* **75**(2), 373–417. DOI: 10.1007/s00285-016-1087-0.

Lowe, M. and Gollub, J. P. (1985). "Pattern selection near the onset of convection: The Eckhaus instability". *Physical Review Letters* **55**(23), 2575–2578. DOI: 10.1103/PhysRevLett.55.2575.

Newell, A. C. and Whitehead, J. A. (1969). "Finite bandwidth, finite amplitude convection". *Journal of Fluid Mechanics* **38**(2), 279–303. DOI: 10.1017/S0022112069000176.

Parra-Rivas, P., Gomila, D., Gelens, L., and Knobloch, E. (2018). "Bifurcation structure of localized states in the Lugiato-Lefever equation with anomalous dispersion". *Physical Review E* **97**(4), 042204. DOI: 10.1103/PhysRevE.97.042204.

Peña, B., Pérez-García, C., Sanz-Anchelergues, A., Míguez, D. G., and Muñuzuri, A. P. (2003). "Transverse instabilities in chemical Turing patterns of stripes". *Physical Review E* **68**(5), 056206. DOI: 10.1103/PhysRevE.68.056206.

Périnet, N., Verschueren, N., and Coulibaly, S. (2017). "Eckhaus instability in the Lugiato-Lefever model". *The European Physical Journal D* **71**(9), 243. DOI: 10.1140/epjd/e2017-80078-9.

Pétrélis, F., Laroche, C., Gallet, B., and Fauve, S. (2015). "Drifting patterns as field reversals". *EPL (Europhysics Letters)* **112**(5), 54007. DOI: 10.1209/0295-5075/112/54007.

Pezzutti, A. D., Vega, D. A., and Villar, M. A. (2011). "Dynamics of dislocations in a two-dimensional block copolymer system with hexagonal symmetry". *Philosophical Transactions of the Royal Society of London A: Mathematical, Physical and Engineering Sciences* **369**(1935), 335–350. DOI: 10.1098/rsta.2010.0269.

Sushchik, M. M. and Tsimring, L. S. (1994). "The Eckhaus instability in hexagonal patterns". *Physica D: Nonlinear Phenomena* **74**(1-2), 90–106. DOI: 10.1016/0167-2789(94)90028-0.

Tsimring, L. S. (1996). "Dynamics of penta-hepta defects in hexagonal patterns". *Physica D: Nonlinear Phenomena* **89**(3-4), 368–380. DOI: 10.1016/0167-2789(95)00222-7.

Tuckerman, L. S. and Barkley, D. (1990). "Bifurcation analysis of the Eckhaus instability". *Physica D: Nonlinear Phenomena* **46**(1), 57–86. DOI: 10.1016/0167-2789(90)90113-4.

Tulumello, E., Lombardo, M. C., and Sammartino, M. (2014). "Cross-diffusion driven instability in a predator-prey system with cross-diffusion". *Acta Applicandae Mathematicae* **132**(1), 621–633. DOI: 10.1007/s10440-014-9935-7.

[a] Università degli Studi della Calabria
Dipartimento di Fisica
Via Pietro Bucci, 87036 Rende, Cosenza, Italy

[b] Università degli Studi di Palermo
Dipartimento di Energia, Ingegneria dell'Informazione e Modelli Matematici
Viale delle Scienze Ed.9, 90128 Palermo, Italy

[c] Università degli Studi di Palermo
Dipartimento di Matematica e Informatica
Via Archirafi 34, 90123 Palermo, Italy

[d] Università degli Studi di Palermo
Dipartimento di Ingegneria Chimica, Gestionale, Informatica, Meccanica
Viale delle Scienze Ed. 8, 90128 Palermo, Italy

* To whom correspondence should be addressed | email: valeria.giunta@unipa.it

Paper contributed to the workshop entitled "Mathematical modeling of self-organizations in medicine, biology and ecology: from micro to macro", which was held at Giardini Naxos, Messina, Italy (18–21 September 2017)
under the patronage of the *Accademia Peloritana dei Pericolanti*
Manuscript received 29 May 2018; published online 30 November 2018